

# Design and Synthesis of Tranylcypromine-Derived LSD1 Inhibitors with Improved hERG and Microsomal Stability Profiles

Published as part of the ACS Medicinal Chemistry Letters special issue "Epigenetics 2022".

Yasuko Koda,<sup>#</sup> Shin Sato,<sup>#</sup> Hirofumi Yamamoto, Hideaki Niwa, Hisami Watanabe, Chiduru Watanabe, Tomohiro Sato, Kana Nakamura, Akiko Tanaka, Mikako Shirouzu, Teruki Honma, Takehiro Fukami, Hiroo Koyama,<sup>\*</sup> and Takashi Umehara<sup>\*</sup>



Cite This: *ACS Med. Chem. Lett.* 2022, 13, 848–854



Read Online

ACCESS |



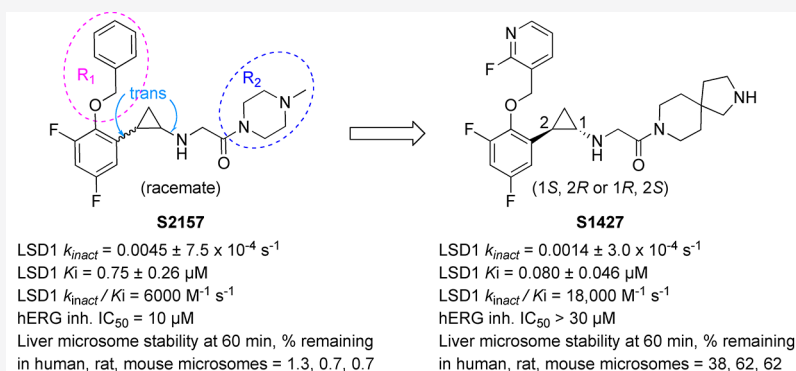
Metrics & More



Article Recommendations



Supporting Information



**ABSTRACT:** Lysine-specific demethylase 1 (LSD1/KDM1A) is a promising therapeutic target for the treatment of cancers. Several derivatives of tranylcypromine (*trans*-2-phenylcyclopropylamine) have been developed as LSD1 inhibitors. One such derivative is **S2157**; however, this compound has a high hERG channel inhibitory activity and a low microsomal stability, making it unsuitable as a drug candidate. Here, using an *in silico* hERG inhibition prediction model, we designed, synthesized, and evaluated a novel series of **S2157** derivatives characterized by modifications of the benzyloxy and piperazine groups. Among the synthesized derivatives, a compound possessing 2-fluoropyridine and 2,8-diaza-spiro[4.5]decane groups (compound **10**) showed the most desirable activities, and its enantiomer, **S1427**, was isolated by the optical resolution of **10**. In addition to potent LSD1 inhibitory activity, **S1427** exhibited desirable hERG channel inhibition and microsomal stability profiles.

**KEYWORDS:** Chromatin, Drug discovery, Epigenetics, Histone, Nucleosome

Lysine-specific demethylase 1 (LSD1 or KDM1A) is a flavin adenine dinucleotide (FAD) dependent demethylase that removes mono- and dimethylated groups at lysine 4 (H3K4) and lysine 9 (H3K9) of histone H3.<sup>1–3</sup> Through its dual function of targeting both H3K4 and H3K9, LSD1 plays a pivotal role in maintaining cellular homeostasis by regulating gene transcription.<sup>4–7</sup> The aberrant expression of LSD1 is present in various cancers, including T-cell acute lymphoblastic leukemia (T-ALL), acute myeloid leukemia, and glioblastoma, which is key in the self-renewal of cancer stem cells.<sup>8–11</sup> The inhibition of LSD1 through gene knockdown or the use of small molecules has been shown to at least partially reduce the proliferation of cancer cells.<sup>12–16</sup>

Tranylcypromine is a nonselective small-molecule inhibitor of FAD-dependent amine oxidases, including LSD1.<sup>17–19</sup> Tranylcypromine exerts its inhibitory activity by forming a covalent adduct with the flavin ring of FAD.<sup>17,18</sup> To develop a

potent LSD1-selective inhibitor, various tranylcypromine derivatives have been synthesized by various groups, including ours.<sup>12,20–24</sup> Our approach has been to modify the phenyl ring and cyclopropylamine of tranylcypromine. For example, we reported one of the earliest LSD1-selective inhibitors, **S2101**, which we synthesized by introducing an *ortho*-benzyloxy group and two *meta*-fluorine atoms to the phenyl ring of tranylcypromine.<sup>25</sup> Subsequently, we identified a more potent LSD1-selective inhibitor, **S2157**, which has (4-methylpiperazin-1-yl)ethanone as the cyclopropylamine substituent.<sup>26</sup> We

**Received:** March 17, 2022

**Accepted:** April 21, 2022

**Published:** April 29, 2022



Table 1. Optimization of the R<sub>1</sub> Group<sup>c</sup>

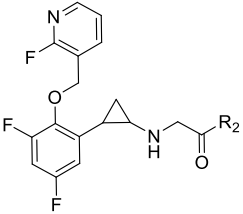
Compound	R <sub>1</sub>	LSD1 IC <sub>50</sub> (μM) <sup>a</sup>	<i>k</i> <sub>inact</sub> (s <sup>-1</sup> ) <sup>a</sup>	<i>K</i> <sub>i</sub> (μM) <sup>a</sup>	<i>k</i> <sub>inact</sub> / <i>K</i> <sub>i</sub> (M <sup>-1</sup> s <sup>-1</sup> )	hERG inhibition at 10 μM	
						Predicted probability (>50%) <sup>b</sup>	Measured value (%) <sup>a</sup>
S2157		0.87 ± 0.023	0.0045 ± 7.5 × 10 <sup>-4</sup>	0.75 ± 0.26	6000	N.D.	51 ± 4
1		2.5 ± 0.028	0.0037 ± 5.3 × 10 <sup>-4</sup>	1.3 ± 0.43	2800	0.53	50 ± 7
2		4.6 ± 0.014	0.0016 ± 2.5 × 10 <sup>-4</sup>	0.47 ± 0.25	3500	0.47	76 ± 16
3		2.7 ± 0.027	0.0029 ± 2.9 × 10 <sup>-4</sup>	1.3 ± 0.36	2300	0.54	>100
4		2.1 ± 0.036	0.0026 ± 2.6 × 10 <sup>-4</sup>	1.4 ± 0.32	1800	0.37	21 ± 3
5		3.1 ± 0.020	0.0039 ± 2.5 × 10 <sup>-4</sup>	2.8 ± 0.50	1400	0.13	46 ± 0.3
6		2.5 ± 0.022	0.0060 ± 1.0 × 10 <sup>-3</sup>	2.9 ± 1.1	2000	0.17	8 ± 3
7		21 ± 0.0077	0.0016 ± 3.9 × 10 <sup>-4</sup>	6.0 ± 3.0	260	0.12	14 ± 9
8		16 ± 0.0066	0.0034 ± 8.4 × 10 <sup>-4</sup>	10 ± 5.4	330	0.20	N.D.

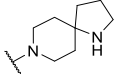
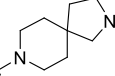
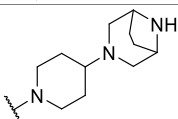
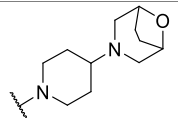
<sup>a</sup>Mean values of three independent experiments. <sup>b</sup>A probability of hERG inhibitory activity >50% at 10 μM was estimated using the AMED hERG SWC model.<sup>30</sup> <sup>c</sup>N.D., not done.

found that S2157 suppressed the growth of human T-ALL cells in a xenoplated mouse cancer model and eradicated leukemia cells from the central nervous system as a result of the compound's high brain penetration.<sup>27</sup> Furthermore, we found that S2157 prevented the teratoma formation of induced pluripotent stem cells *in vivo*.<sup>28</sup>

Although we demonstrated that S2157 has potent pharmacological effects against T-ALL cells due to its LSD1-

inhibiting activity, there is still room for improvement in its other properties. For instance, its liver microsomal stability and hERG channel inhibition profile are less than optimal; the percentage of S2157 that remains after 60 min of incubation with human, rat, or mouse microsomes is below 10%, and the half-maximum inhibitory concentration of the hERG channel (hERG IC<sub>50</sub>) is approximately 10 μM (Table 1). Here, with the help of an *in silico* hERG inhibition prediction model,<sup>30</sup> we

Table 2. Optimization of the R<sub>2</sub> Group


Compound	R <sub>2</sub>	LSD1 IC <sub>50</sub> (μM) <sup>a</sup>	k <sub>inact</sub> (s <sup>-1</sup> ) <sup>a</sup>	K <sub>i</sub> (μM) <sup>a</sup>	k <sub>inact</sub> /K <sub>i</sub> (M <sup>-1</sup> s <sup>-1</sup> )	Liver microsomal stability (% remaining after 60 min) <sup>b</sup> human/rat/mouse	hERG (% inhibition) at 10 μM <sup>a</sup>
9		0.75 ± 0.0037	0.0014 ± 3.9 × 10 <sup>-4</sup>	0.19 ± 0.10	7500	41 / 20 / 42	62 ± 13
10		1.0 ± 0.0026	0.0014 ± 4.2 × 10 <sup>-4</sup>	0.22 ± 0.13	6300	44 / 56 / 73	10 ± 5
11		1.4 ± 0.066	0.0034 ± 7.6 × 10 <sup>-4</sup>	0.72 ± 0.44	4700	0 / 24 / 25	23 ± 14
12		3.7 ± 0.025	0.0019 ± 1.7 × 10 <sup>-4</sup>	0.73 ± 0.24	2600	0 / 0 / 0	32 ± 4

<sup>a</sup>Mean values of three independent experiments.

rationally designed, synthesized, and evaluated a series of S2157 derivatives with improved drug metabolism, pharmacokinetics, and off-target activity profiles.

To help identify compounds with low hERG inhibitory activities and high LSD1 inhibitory activities, we used a recent *in silico* hERG inhibition prediction model (the AMED hERG SVM model)<sup>29</sup> (see the Supporting Information for details). The two parent compounds used for virtual compound generation are shown in Figure S1. The predicted hERG channel inhibition probabilities of the virtual compounds generated from compounds A and B in Figure S1 are respectively shown in Tables S1 and S2. After considering the results obtained with the model, as well as the drug-likeness and the synthetic accessibility, we synthesized a series of S2157 derivatives with modifications at one of two positions (R<sub>1</sub> and R<sub>2</sub>; see Tables 1 and 2, respectively, and Supporting Information Scheme 1). The LSD1 and hERG inhibitory activities of the derivatives were measured *in vitro* using the peroxidase-coupled reaction method<sup>30</sup> and the automated patch-clamp assay in hERG-expressing HEK293 cells,<sup>31</sup> respectively (see the Supporting Information for details).

The introduction of various substituents to the phenyl group of S2157 was accomplished by subjecting 2,4-difluorophenol to an addition–elimination reaction,<sup>25</sup> followed by cyclopropanation between ethyldiazoacetate and the allyl group of the phenyl group, hydrolysis of the ethylester, and Curtius rearrangement; the derivatives obtained were mainly *trans*-2-aryl-cyclopropyl-1-amine derivatives. All the substitutions at the R<sub>1</sub> and R<sub>2</sub> positions were accomplished following a

literature procedure,<sup>25</sup> and the conditions are summarized in Supporting Information Scheme 1.

Early in the study (see Table S3 and the Supporting Information for details), compound 1 was found to exhibit a slightly improved microsomal stability (liver microsome stability at 60 min; 5.1%, 13%, and 4.7% remaining in human, rat, and mouse microsomes, respectively) compared to that of S2157 (1.3%, 0.7%, and 0.7%), albeit with an approximately twofold reduction of its LSD1-inhibiting potency (K<sub>i</sub> = 1.3 ± 0.43 μM versus 0.75 ± 0.26 μM, respectively; k<sub>inact</sub>/K<sub>i</sub> = 2800 M<sup>-1</sup> s<sup>-1</sup> versus 6000 M<sup>-1</sup> s<sup>-1</sup>, respectively; see Table 1). We therefore decided to start our structural modifications using 1. Table 1 summarizes our optimization of the R<sub>1</sub> group, where the R<sub>2</sub> group was fixed as *N*-methoxyethyl piperazine.

As compared with 1, extending the methylene linkage between the phenyl and aryl groups in compounds 2 and 3 did not reduce the hERG inhibitory activity. In contrast, substituting 2-fluoropyridine at the R<sub>1</sub> position (4) resulted in a marked reduction in the hERG inhibitory activity without a reduction in the LSD1 inhibitory activity. Compound 6 with a pyrazole at R<sub>1</sub> showed an overall profile that was comparable to that of 4, but mild degradation was observed during high-performance liquid chromatography analysis. Overall, a correlation (R<sup>2</sup> = 0.54) was observed between the predicted and measured hERG channel inhibitory activities (Figure S2). Thus, this prediction may be useful for compound screening, but the actual measurement of the hERG inhibitory activities of the selected compounds is still necessary.

Considering that the introduction of 2-fluoropyridine at the R<sub>1</sub> position resulted in a reduction of the hERG channel inhibitory activity, we analyzed the binding modes of compounds **4** and **5** (both of which possessed a 2-fluoropyridine group) toward LSD1 by X-ray crystallography. To understand the binding modes of **4** and **5** toward LSD1, we determined their cocrystal structures at 2.94 and 2.91 Å, respectively (Table S4). The electron density maps for **4** (Figure 1A) and **5** (Figure S3-A) revealed that the N-

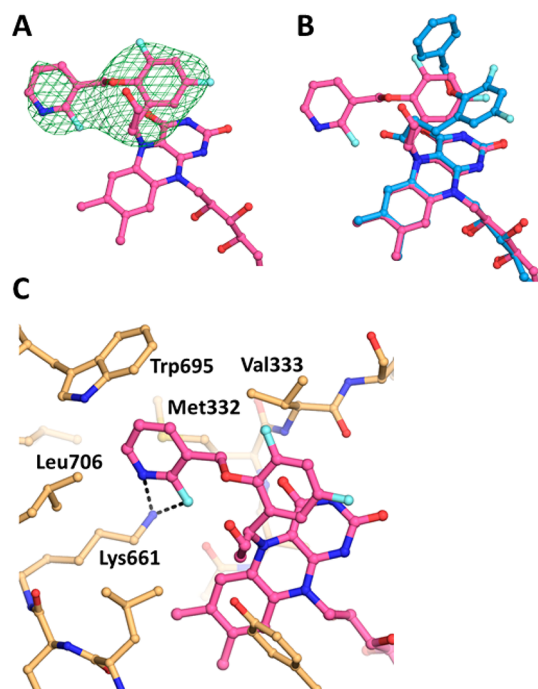


**Figure 1.** Crystal structure analysis of LSD1 complexed with **4**. (A) Electron density map of the FAD-**4** adduct. The *mFo-DFc* map at +2.5  $\sigma$ , which was calculated without the compound portion of the adduct, is shown as a green mesh. (B) Superimposition of the structures of the FAD-**4** and FAD-**S2157** adducts. The FAD-**4** and FAD-**S2157** adducts are shown as magenta and cyan sticks, respectively. The nitrogen, oxygen, and fluorine atoms are shown in dark blue, red, and light blue, respectively. (C) Interactions of the FAD-**4** adduct. The adduct is shown as in panel B, and the protein residues are shown as orange sticks.

methoxyethyl piperazine portions (R<sub>2</sub>) of **4** and **5** were lacking in the crystal structures, which was consistent with observations for other N-alkylated derivatives, including **S2157** (PDB ID 6KGP).<sup>26</sup>

Interestingly, the adducts formed between FAD and these derivatives were different from that formed between FAD and **S2157**.<sup>26</sup> First, the covalent bond-forming carbon atom in the cyclopropane of the derivatives was different. In the FAD-**S2157** adduct, a carbonyl carbon of **S2157** was bonded to N5 of FAD, whereas in the adducts with **4** or **5** a carbon attached to the phenyl ring that was bonded to FAD. Second, in the FAD-**S2157** adduct, the benzyloxy group of **S2157** extended toward the opening of the catalytic cavity. In contrast, in the FAD adducts with **4** and **5**, the fluoropyridine groups of **4** and **5** extended toward a side pocket in the catalytic cavity formed by Met332, Trp695, Leu706, and Lys661 (Figure 1B and C, respectively). In addition, atoms in the benzyloxy group of **S2157** did not interact with the side-chain nitrogen atom of Lys661, whereas the fluorine and nitrogen atoms of the fluoropyridine ring of **4** and the fluorine atom of **5** did interact with that atom (Figures 1C and S3B). Furthermore, due to the steric hindrance caused by the fluoropyridine ring, the conformations of the Met332 side-chain in the structures of LSD1-**4** (Figure 1C) and LSD1-**5** (Figure S3B) were different from that in LSD1-**S2157**. We attribute these differences to the interactions of the different R<sub>1</sub> moieties with the surrounding residues, including Lys661, and the effects of the different R<sub>2</sub> moieties on the position of the derivative with respect to the FAD structure before the formation of the covalent bond.

Table 2 summarizes our optimization of the R<sub>2</sub> group, where R<sub>1</sub> was fixed as the moiety used in compound **4**. The substitution of spiro-fused pyrrolo-piperidines at the R<sub>2</sub> position (**9** and **10**) resulted in improvements in the LSD1-inhibitory activity ( $k_{\text{inact}}/K_i = 7500$  and  $6300 \text{ M}^{-1} \text{ s}^{-1}$ , respectively) and the liver microsomal stability as compared with those of **4** and **S2157**, although the hERG-inhibitory activity of the derivatives was sensitive to the position of the pyrrole nitrogen. The substitution of bicyclic piperazine and piperidine at the R<sub>2</sub> position (**11** and **12**, respectively) also resulted in a low hERG-inhibitory activity, but the liver microsomal stability was poor. With these findings in mind, compound **10** was selected for enantiomeric characterization. As a class, **S2157** derivatives contain a chiral structural motif at the 1,2-*trans*-substituted cyclopropyl group. Therefore, the

**Table 3.** Summary of the Activities of the Enantiomers of **10**

compound	chiral form	LSD1 IC <sub>50</sub> ( $\mu\text{M}$ ) <sup>a</sup>	$k_{\text{inact}}$ ( $\text{s}^{-1}$ ) <sup>a</sup>	$K_i$ ( $\mu\text{M}$ ) <sup>a</sup>	$k_{\text{inact}}/K_i$ ( $\text{M}^{-1} \text{ s}^{-1}$ )	liver microsomal stability (% remaining after 60 min, human/rat/mouse)	hERG inhibition IC <sub>50</sub> ( $\mu\text{M}$ ) <sup>a</sup>
<b>10a</b> ( <b>S1427</b> )	(-)	0.39 ± 0.0040	0.0014 ± 3.0 × 10 <sup>-4</sup>	0.080 ± 0.046	18 000	38/62/62	>30
<b>10b</b> ( <b>S1428</b> )	(+)	28 ± 0.0019	0.00076 ± 1.1 × 10 <sup>-4</sup>	4.5 ± 1.8	170	45/55/73	>30

<sup>a</sup>Mean values of three independent experiments.

optical resolution of **10** was achieved by chiral column separation to afford **10a** (**S1427**) and **10b** (**S1428**) with >95% enantiomeric excess. Despite several attempts, we were unable to successfully determine the absolute stereochemistry.

Table 3 summarizes the *in vitro* activities of enantiomers **10a** (**S1427**) and **10b** (**S1428**). **S1427** showed a value for  $k_{\text{inact}}/K_i$  against LSD1 more than 100× higher than that of **S1428**, but both enantiomers exhibited similar liver microsomal stabilities and hERG inhibition profiles. In addition to **S2157**,<sup>26</sup> both **S1427** and **S1428** exhibited selectivity for LSD1 over monoamine oxidase (MAO)-A and MAO-B, and their  $K_i$  values for MAO-A and MAO-B were both above 250  $\mu\text{M}$  (Table S5). X-ray crystallography confirmed that **S1427** formed an adduct with FAD (Figure 2 and Table S4) in a manner almost identical to that of **4** (Figure 1C), suggesting that differences at the R<sub>2</sub> position did not affect the adduct structure.

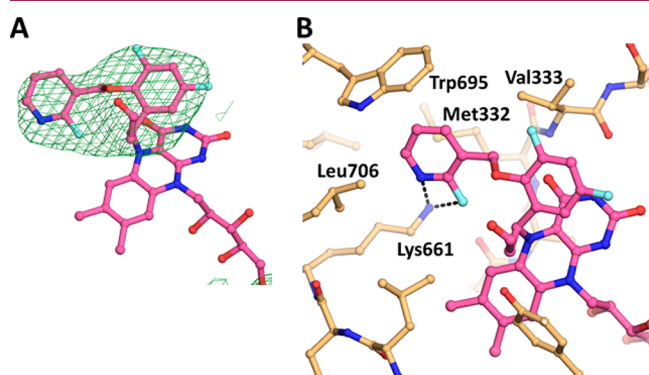


**Figure 2.** Crystal structure analysis of LSD1 complexed with **S1427**. (A) Electron density map of the FAD–**S1427** adduct. (B) Interactions of the FAD–**S1427** adduct. Figures are depicted as in Figure 1A and C.

Subsequently, we conducted a mouse pharmacokinetics study using **S1427** and **S2157** (Table 4). Significantly more

**Table 4.** Comparison of the Pharmacokinetic Profiles of **S2157** and **S1427**<sup>a</sup>

parameter	<b>S2157</b>	<b>S1427 (10a)</b>
AUC <sub>0–∞</sub> ( $\mu\text{M}\cdot\text{h}$ )	0.98	5.09
C <sub>max</sub> ( $\mu\text{M}$ )	0.96	3.03
T <sub>max</sub> (h)	0.25	0.50
T <sub>1/2</sub> (h)	0.95	3.90

<sup>a</sup>Compounds were administered via a single intraperitoneal injection at a dosage of 10 mg/5 mL per kilogram ( $n = 3$ ) to an ICR-strain mouse (eight weeks old, male).

exposure (area under the concentration–time curve from 0 to the last measurement; AUC<sub>0–∞</sub>), a higher maximum serum concentration, and a longer serum half-life were observed for **S1427** compared with **S2157** (Table 4). Finally, we treated human T-ALL Jurkat cells with **S1427** or **S1428** and examined their effects on LSD1-dependent transcriptional regulation. As expected, the expression of *NOTCH3*, which is one of the genes downregulated in Jurkat cells by the chemical inhibition of LSD1,<sup>27</sup> was significantly reduced by treatment with **S1427**, as was observed with **S2157** (Figure 3). However, the effect of the less-active enantiomer, **S1428**, was comparable with that of the control (DMSO-treated cells).

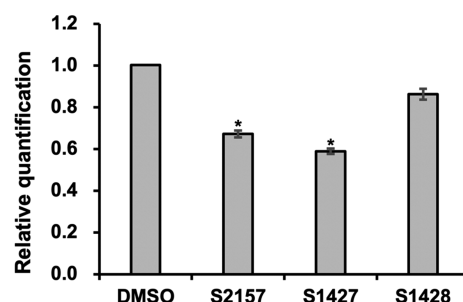


**Figure 3.** Downregulation of *NOTCH3* expression by **S1427**. Jurkat cells were cultured with 10  $\mu\text{M}$  test compound for 12 h. The expression level of *NOTCH3* normalized to *GAPDH* was quantified by real-time PCR and statistically analyzed using the independent-samples one-sided *t* test ( $*p < 0.01$ ). Data are presented as the mean  $\pm$  SD ( $n = 3$ ).

In conclusion, a systematic SAR study that used an *in silico* hERG channel inhibition prediction model and started from the tranlylcypromine derivative **S2157** led to the identification of the novel LSD1 inhibitor **S1427**. Compared with the parent compound, **S1427** had triple the  $k_{\text{inact}}/K_i$  value against LSD1 ( $k_{\text{inact}}/K_i = 18,000$  vs  $6000 \text{ M}^{-1} \text{ s}^{-1}$ ), a lower hERG-inhibitory activity ( $\text{IC}_{50} > 30 \mu\text{M}$  vs  $10 \mu\text{M}$ ), and a significantly better liver microsomal stability *in vitro*. Together with the newly obtained cocrystal X-ray structures, the accumulated knowledge of the SARs and off-target profiles of the tranlylcypromine derivatives is expected to offer valuable insights for the future development of LSD1 inhibitors as therapeutic agents.

## ■ ASSOCIATED CONTENT

### Supporting Information

The Supporting Information is available free of charge at <https://pubs.acs.org/doi/10.1021/acsmmedchemlett.2c00120>.

*In silico* docking, chemistry, and biological evaluations (PDF)

## ■ AUTHOR INFORMATION

### Corresponding Authors

**Takashi Umehara** – Laboratory for Epigenetics Drug Discovery, RIKEN Center for Biosystems Dynamics Research, Tsurumi, Yokohama 230-0045, Japan; Drug Discovery Structural Biology Platform Unit, RIKEN Center for Biosystems Dynamic Research, Yokohama, Kanagawa 230-0045, Japan; [orcid.org/0000-0003-3464-2960](https://orcid.org/0000-0003-3464-2960); Email: [takashi.umehara@riken.jp](mailto:takashi.umehara@riken.jp)

**Hiroo Koyama** – Drug Discovery Chemistry Platform Unit, Drug Discovery Seed Compounds Exploratory Unit, Chemical Genomics Research Group, RIKEN Center for Sustainable Resource Science, Wako, Saitama 351-0198, Japan; Email: [hiroo.koyama@riken.jp](mailto:hiroo.koyama@riken.jp)

### Authors

**Yasuko Koda** – Drug Discovery Chemistry Platform Unit, Drug Discovery Seed Compounds Exploratory Unit, Chemical Genomics Research Group, RIKEN Center for Sustainable Resource Science, Wako, Saitama 351-0198, Japan; [orcid.org/0000-0001-7666-9489](https://orcid.org/0000-0001-7666-9489)

**Shin Sato** – Laboratory for Epigenetics Drug Discovery, RIKEN Center for Biosystems Dynamics Research, Tsurumi, Yokohama 230-0045, Japan; Drug Discovery Structural

Biology Platform Unit, RIKEN Center for Biosystems Dynamic Research, Yokohama, Kanagawa 230-0045, Japan  
**Hirofumi Yamamoto** – Drug Discovery Chemistry Platform Unit, Drug Discovery Seed Compounds Exploratory Unit, Chemical Genomics Research Group, RIKEN Center for Sustainable Resource Science, Wako, Saitama 351-0198, Japan

**Hideaki Niwa** – Laboratory for Epigenetics Drug Discovery, RIKEN Center for Biosystems Dynamics Research, Tsurumi, Yokohama 230-0045, Japan; Drug Discovery Structural Biology Platform Unit, RIKEN Center for Biosystems Dynamic Research, Yokohama, Kanagawa 230-0045, Japan;  
[orcid.org/0000-0001-9544-9350](https://orcid.org/0000-0001-9544-9350)

**Hisami Watanabe** – Laboratory for Epigenetics Drug Discovery, RIKEN Center for Biosystems Dynamics Research, Tsurumi, Yokohama 230-0045, Japan; Drug Discovery Structural Biology Platform Unit, RIKEN Center for Biosystems Dynamic Research, Yokohama, Kanagawa 230-0045, Japan

**Chiduru Watanabe** – Drug Discovery Computational Chemistry Platform Unit, RIKEN Center for Biosystems Dynamics Research, Tsurumi, Yokohama 230-0045, Japan;  
[orcid.org/0000-0002-0742-3896](https://orcid.org/0000-0002-0742-3896)

**Tomohiro Sato** – Drug Discovery Computational Chemistry Platform Unit, RIKEN Center for Biosystems Dynamics Research, Tsurumi, Yokohama 230-0045, Japan;  
[orcid.org/0000-0002-0660-5559](https://orcid.org/0000-0002-0660-5559)

**Kana Nakamura** – Drug Discovery Structural Biology Platform Unit, RIKEN Center for Biosystems Dynamic Research, Yokohama, Kanagawa 230-0045, Japan

**Akiko Tanaka** – Drug Discovery Structural Biology Platform Unit, RIKEN Center for Biosystems Dynamic Research, Yokohama, Kanagawa 230-0045, Japan

**Mikako Shirouzu** – Drug Discovery Structural Biology Platform Unit, RIKEN Center for Biosystems Dynamic Research, Yokohama, Kanagawa 230-0045, Japan

**Teruki Honma** – Drug Discovery Computational Chemistry Platform Unit, RIKEN Center for Biosystems Dynamics Research, Tsurumi, Yokohama 230-0045, Japan;  
[orcid.org/0000-0003-3761-9504](https://orcid.org/0000-0003-3761-9504)

**Takehiro Fukami** – RIKEN Program for Drug Discovery and Medical Technology Platforms, Wako, Saitama 351-0198, Japan

Complete contact information is available at:  
<https://pubs.acs.org/10.1021/acsmchemlett.2c00120>

### Author Contributions

#These authors contributed equally to this work.

### Notes

The authors declare no competing financial interest.

### ACKNOWLEDGMENTS

We thank the staff of beamline BL26B2 at SPring-8 (Hyogo, Japan) and beamline X06DA at Swiss Light Source (Villigen, Switzerland) for their help with the collection of the X-ray diffraction data and Dr. Keiji Ogura (RIKEN) for his technical support and useful discussion about the *in silico* hERG inhibition prediction model. This study was supported by the RIKEN Program for Drug Discovery and Medical Technology Platforms, the Japan Society for the Promotion of Science (20H03388 and 20K21406), and the Platform Project for Supporting Drug Discovery and Life Science

Research (Basis for Supporting Innovative Drug Discovery and Life Science Research) from the Japan Agency for Medical Research and Development (AMED) under Grant JP21am0101113. This study was also partially supported by the AMED Drug Discovery Informatics project.

### REFERENCES

- (1) Shi, Y.; Lan, F.; Matson, C.; Mulligan, P.; Whetstone, J.; Cole, P.; Casero, R.; Shi, Y. Histone demethylation mediated by the nuclear amine oxidase homolog LSD1. *Cell* **2004**, *119*, 941–953.
- (2) Metzger, E.; Wissmann, M.; Yin, N.; Muller, J.; Schneider, R.; Peters, A.; Gunther, T.; Buettner, R.; Schule, R. LSD1 demethylates repressive histone marks to promote androgen-receptor-dependent transcription. *Nature* **2005**, *437*, 436–439.
- (3) Mosammammarast, N.; Shi, Y. Biochemical and molecular mechanisms of histone demethylases. *Annu. Rev. Biochem.* **2010**, *79*, 155–179.
- (4) Varier, R.; Timmers, H. Histone lysine methylation and demethylation pathways in cancer. *Biochim. Biophys. Acta. Rev. Cancer* **2011**, *1815*, 75–89.
- (5) Lan, F.; Nottke, A.; Shi, Y. Mechanisms involved in the regulation of histone lysine demethylases. *Curr. Opin. Cell Biol.* **2008**, *20*, 316–325.
- (6) Amente, S.; Lania, L.; Majello, B. The histone LSD1 demethylase in stemness and cancer transcription programs. *Biochim. Biophys. Acta. Gene Regul Mech* **2013**, *1829*, 981–986.
- (7) Forneris, F.; Binda, C.; Battaglioli, E.; Mattevi, A. LSD1: Oxidative chemistry for multifaceted functions in chromatin regulation. *Trends Biochem. Sci.* **2008**, *33*, 181–189.
- (8) Wada, T.; Koyama, D.; Kikuchi, J.; Honda, H.; Furukawa, Y. Overexpression of the shortest isoform of histone demethylase LSD1 primes hematopoietic stem cells for malignant transformation. *Blood* **2015**, *125*, 3731–3746.
- (9) Schenk, T.; Chen, W.; Gollner, S.; Howell, L.; Jin, L.; Hebestreit, K.; Klein, H.; Popescu, A.; Burnett, A.; Mills, K.; Casero, R.; Marton, L.; Woster, P.; Minden, M.; Dugas, M.; Wang, J.; Dick, J.; Muller-Tidow, C.; Petrie, K.; Zelent, A. Inhibition of the LSD1 (KDM1A) demethylase reactivates the all-trans-retinoic acid differentiation pathway in acute myeloid leukemia. *Nat. Med.* **2012**, *18*, 605–611.
- (10) Harris, W.; Huang, X.; Lynch, J.; Spencer, G.; Hitchin, J.; Li, Y.; Ciceri, F.; Blaser, J.; Greystoke, B.; Jordan, A.; Miller, C.; Ogilvie, D.; Somerville, T. The histone demethylase KDM1A sustains the oncogenic potential of MLL-AF9 leukemia stem cells. *Cancer Cell* **2012**, *21*, 473–487.
- (11) Suva, M.; Rheinbay, E.; Gillespie, S.; Patel, A.; Wakimoto, H.; Rabkin, S.; Riggi, N.; Chi, A.; Cahill, D.; Nahed, B.; Curry, W.; Martuza, R.; Rivera, M.; Rossetti, N.; Kasif, S.; Beik, S.; Kadri, S.; Tirosh, I.; Wortman, I.; Shalek, A.; Rozenblatt-Rosen, O.; Regev, A.; Louis, D.; Bernstein, B. Reconstructing and reprogramming the tumor-propagating potential of glioblastoma stem-like cells. *Cell* **2014**, *157*, 580–594.
- (12) Niwa, H.; Umehara, T. Structural insight into inhibitors of flavin adenine dinucleotide-dependent lysine demethylases. *Epigenetics* **2017**, *12*, 340–352.
- (13) Morera, L.; Lübbert, M.; Jung, M. Targeting histone methyltransferases and demethylases in clinical trials for cancer therapy. *Clinical Epigenetics* **2016**, *8*, 57.
- (14) Cole, P. Chemical probes for histone-modifying enzymes. *Nat. Chem. Biol.* **2008**, *4*, 590–597.
- (15) McAllister, T.; England, K.; Hopkinson, R.; Brennan, P.; Kawamura, A.; Schofield, C. Recent progress in histone demethylase inhibitors. *J. Med. Chem.* **2016**, *59*, 1308–1329.
- (16) Zheng, Y.; Ma, J.; Wang, Z.; Li, J.; Jiang, B.; Zhou, W.; Shi, X.; Wang, X.; Zhao, W.; Liu, H. A systematic review of histone lysine-specific demethylase 1 and its inhibitors. *Med. Res. Rev.* **2015**, *35*, 1032–1071.

- (17) Lee, M.; Wynder, C.; Schmidt, D.; McCafferty, D.; Shiekhhattar, R. Histone H3 lysine 4 demethylation is a target of nonselective antidepressive medications. *Chem. Biol.* **2006**, *13*, 563–567.
- (18) Schmidt, D.; McCafferty, D. *trans*-2-Phenylcyclopropylamine is a mechanism-based inactivator of the histone demethylase LSD1. *Biochemistry* **2007**, *46*, 4408–4416.
- (19) Fioravanti, R.; Romanelli, A.; Mautone, N.; Di Bello, E.; Rovere, A.; Corinti, D.; Zwergel, C.; Valente, S.; Rotili, D.; Botrugno, O.; Dessanti, P.; Vultaggio, S.; Vianello, P.; Cappa, A.; Binda, C.; Mattevi, A.; Minucci, S.; Mercurio, C.; Varasi, M.; Mai, A. Tranylcyproline-Based LSD1 Inhibitors: Structure-Activity Relationships, Antiproliferative Effects in Leukemia, and Gene Target Modulation. *ChemMedChem*. **2020**, *15*, 643–658.
- (20) Neelamegam, R.; Ricq, E.; Malvaez, M.; Patnaik, D.; Norton, S.; Carlin, S.; Hill, I.; Wood, M.; Haggarty, S.; Hooker, J. Brain-Penetrant LSD1 Inhibitors Can Block Memory Consolidation. *ACS Chem. Neurosci.* **2012**, *3*, 120–128.
- (21) Khan, M. N. A.; Tsumoto, H.; Itoh, Y.; Ota, Y.; Suzuki, M.; Ogasawara, D.; Nakagawa, H.; Mizukami, T.; Miyata, N.; Suzuki, T. Design, synthesis, and biological activity of *N*-alkylated analogue of NCL1, a selective inhibitor of lysine-specific demethylase 1. *MedChemComm* **2015**, *6*, 407–412.
- (22) Zhou, C.; Wu, F.; Lu, L.; Wei, L.; Pai, E.; Yao, Y.; Song, Y. Structure activity relationship and modeling studies of inhibitors of lysine specific demethylase 1. *PLoS One* **2017**, *12*, e0170301.
- (23) Schulz-Fincke, J.; Hau, M.; Barth, J.; Robaa, D.; Willmann, D.; Kurner, A.; Haas, C.; Greve, G.; Haydn, T.; Fulda, S.; Lubbert, M.; Ludeke, S.; Berg, T.; Sippl, W.; Schule, R.; Jung, M. Structure-activity studies on *N*-Substituted tranylcyproline derivatives lead to selective inhibitors of lysine specific demethylase 1 (LSD1) and potent inducers of leukemic cell differentiation. *Eur. J. Med. Chem.* **2018**, *144*, 52–67.
- (24) Maes, T.; Mascaro, C.; Tirapu, I.; Estiarte, A.; Ciceri, F.; Lunardi, S.; Guibourt, N.; Perdones, A.; Lufino, M.; Somervaille, T.; Wiseman, D.; Duy, C.; Melnick, A.; Willekens, C.; Ortega, A.; Martinell, M.; Valls, N.; Kurz, G.; Fyfe, M.; Castro-Palomino, J.; Buesa, C. ORY-1001, a potent and selective covalent KDM1A inhibitor, for the treatment of acute leukemia. *Cancer Cell* **2018**, *33*, 495–511.
- (25) Mimasu, S.; Umezawa, N.; Sato, S.; Higuchi, T.; Umehara, T.; Yokoyama, S. Structurally designed *trans*-2-phenylcyclopropylamine derivatives potentially inhibit histone demethylase LSD1/KDM1. *Biochemistry* **2010**, *49*, 6494–6503.
- (26) Niwa, H.; Sato, S.; Handa, N.; Sengoku, T.; Umehara, T.; Yokoyama, S. Development and structural evaluation of *N*-alkylated *trans*-2-phenylcyclopropylamine-based LSD1 inhibitors. *ChemMedChem*. **2020**, *15*, 787–793.
- (27) Saito, S.; Kikuchi, J.; Koyama, D.; Sato, S.; Koyama, H.; Osada, N.; Kuroda, Y.; Akahane, K.; Inukai, T.; Umehara, T.; Furukawa, Y. Eradication of central nervous system leukemia of T-cell origin with a brain-permeable LSD1 Inhibitor. *Clin. Cancer Res.* **2019**, *25*, 1601–1611.
- (28) Osada, N.; Kikuchi, J.; Umehara, T.; Sato, S.; Urabe, M.; Abe, T.; Hayashi, N.; Sugitani, M.; Hanazono, Y.; Furukawa, Y. Lysine-specific demethylase 1 inhibitors prevent teratoma development from human induced pluripotent stem cells. *Oncotarget* **2018**, *9*, 6450–6462.
- (29) Ogura, K.; Sato, T.; Yuki, H.; Honma, T. Support Vector Machine model for hERG inhibitory activities based on the integrated hERG database using descriptor selection by NSGA-II. *Sci. Rep.* **2019**, *9*, 12220.
- (30) Kitagawa, H.; Kikuchi, M.; Sato, S.; Watanabe, H.; Umezawa, N.; Kato, M.; Hisamatsu, Y.; Umehara, T.; Higuchi, T. Structure-based identification of potent lysine-specific demethylase 1 inhibitor peptides and temporary cyclization to enhance proteolytic stability and cell growth-inhibitory activity. *J. Med. Chem.* **2021**, *64*, 3707–3719.
- (31) Golden, A.; Li, N.; Chen, Q.; Lee, T.; Nevill, T.; Cao, X.; Johnson, J.; Erdemli, G.; Ionescu-Zanetti, C.; Urban, L.; Holmqvist, M. IonFlux: A microfluidic patch clamp system evaluated with human Ether-a-go-go related gene channel physiology and pharmacology. *Assay Drug Dev. Technol.* **2011**, *9*, 608–619.